

# X-RAY OBSERVATIONS OF V4641 SGR (= SAX J1819.3-2525) DURING THE BRIEF AND VIOLENT OUTBURST OF 2003

Dipankar Maitra and Charles D. Bailyn

*Yale University, Department of Astronomy, P.O.Box 208101, New Haven, CT, 06520-8101*

`maitra,bailyn@astro.yale.edu`

## ABSTRACT

We present the results of detailed analysis of pointed X-ray observations by RXTE PCA/HEXTE of the black hole X-ray binary (BHXRb) system V4641 Sgr (= SAX J1819.3-2525) during its outburst of August 2003. Soft X-ray (3-20 keV) flux variations by factors of 10 or more on timescales of minutes or shorter were seen. The rapid and strong variability of this source sets it apart from typical XRBs. In spite of large luminosity fluctuations, the spectral state of the source did not change significantly during the dwells which suggests that the physical emission processes did not change much during the observations. The energy spectra during the dwells were dominated by a hard Comptonized powerlaw component, indicative of the canonical low/hard state observed in other BHXRbS. No soft thermal component was found in three out of the four RXTE pointings. However spectral deconvolution of the observation with largest average luminosity suggests an obscured, hot accretion disk. During one of the observations we detected a short term ( $\sim 100$ s) soft X-ray dropout which is apparently due to variability in the observed column density. Strong Fe  $K\alpha$  fluorescent emission line near 6.5 keV was detected with large equivalent widths in the range of 700 - 1000eV. In the temporal domain, the Fourier power spectra were dominated by red noise below a few Hz. Poisson noise dominated at higher frequencies and no high frequency features were detected. The strong Comptonized spectra, broad iron emission line, absence of disk component in the spectra, absence of any timing variability above few Hz and occasional large changes in the column density along the line-of-sight, all support an enshrouded black hole with occasional outflow and a very dynamic environment.

*Subject headings:* accretion, accretion disks — stars: black holes — X-rays: binaries — individual (V4641 Sgr)

## 1. Introduction

Outbursts in transient X-ray binary systems typically span orders of magnitude in luminosity and mass accretion rate. This allows one to study accretion physics over a wide range as well as general relativity in the strong field limit. During a complete outburst cycle, the sources exhibit a multitude of states that have very different spectral and temporal characteristics from each other. Two canonical states that most transients seem to go through are (i) a hard powerlaw dominated state with high rms variability in the lightcurve, termed the *low/hard* state and (ii) the *high/soft* or *thermal dominant* state with soft photon dominated spectra from the accretion disk and little rms variability. Sometime a very high state with steep powerlaw is also seen (see Tanaka & Lewin (1995) and McClintock & Remillard (2005) for a recent review).

V4641 Sagittarii (SAX J1819.3-2525) was discovered by Goranskij (1978) when it went through an optical flare and hence it was categorized as an irregular optical variable. Initially this system was confused with another neighboring long-period variable called GM Sgr, therefore many old literature erroneously refer to GM Sgr as the optical counterpart of the strong X-ray source. The system was first detected in X-ray wavelengths in February 1999, independently by *BeppoSAX* (in 't Zand et al. 1999) and RXTE (Markwardt et al. 1999) and designated as SAX J1819.3-2525. V4641 Sgr is presently known to be a compact binary system harboring a  $9.61^{+2.08}_{-0.88}M_{\odot}$  black hole candidate and a  $6.53^{+1.6}_{-1.03}M_{\odot}$  B9 secondary star, with an orbital period of  $2.81730 \pm 0.00001$  days (Orosz et al. 2001). Orosz et al. (2001) estimated the distance to the system between 7.4 to 12.3 kpc and an orbital inclination between  $60^{\circ} - 70^{\circ}$ . We have used an inclination of  $65^{\circ}$  and a distance of 10 kpc for all the calculations in this paper.

During the outburst of V4641 Sgr in 1999, RXTE observations showed flaring X-ray activity with Super-Eddington luminosity (Wijnands & van der Klis 2000; Revnivtsev et al. 2002) on Sep 15. Rapid variability in optical brightness were also reported (Stubbings & Pearce 1999; Uemura et al. 2002) during this outburst. Radio observations during the outburst revealed a marginally resolved structure (Hjellming et al. 2000). The inferred superluminal proper motions of the radio structure ( $\gtrsim 0.22$  arcseconds per day) were attributed to relativistic motion of a radio jet. This led to its classification as a possible galactic microquasar like GRS 1915+105 (Mirabel & Rodriguez 1994) and GRO 1655-40 (Tingay et al. 1995; Hjellming & Rupen 1995). Based on the X-ray observations, Revnivtsev et al. (2002) suggested the formation of an extended envelope/outflow around the source during the outburst. Optical spectroscopy by Charles et al. (1999) also suggest the presence of strong wind.

Since the 1999 outburst, activity from the source has been reported in 2000 (Hjellming

2000), 2002 (Uemura et al. 2004), 2003 (Buxton et al. 2003) and 2004 (Swank 2004). In all cases, the entire span of the outburst cycles for this source is much shorter than that of typical compact transient systems. Also, V4641 Sgr does not exhibit a typical *Fast Rise and Exponential Decay* (FRED) (Chen et al. 1997) lightcurve profile during the outburst.

In 2003, signs of activity was first noted by VSNET<sup>1</sup> group on Aug 01, 2003 and shortly thereafter by the *Small and Moderate Aperture Research Telescope System* (SMARTS)<sup>2</sup> consortium telescopes at Cerro Tololo Inter-American Observatory (CTIO) in Chile (Buxton et al. 2003). Subsequent multiwavelength observations showed that the source was active in X-rays (Bailyn et al. 2003) and radio (Rupen et al. 2003) as well. As is characteristic for this enigmatic source, rapid time variability was observed in data obtained from radio, optical as well as X-rays. The observed X-ray spectrum was very hard in nature, i.e. a strong contribution of hard X-rays were seen compared to the soft X-ray flux. The source of the hard X-ray radiation is believed to be either inverse Compton scattering of soft thermal photons from the accretion disk (Sunyaev & Titarchuk 1980) and/or synchrotron emission from a jet (Markoff et al. 2001). Broad and strong iron fluorescent emission lines near 6.5 keV were observed. These lines are thought to be produced by reprocessing of hard X-rays impinging on cold matter, usually the accretion disk (George & Fabian 1991; Reynolds & Nowak 2003), where principal factors that causes the line to broaden are strong gravitational field near the compact source and relativistic motion of the radiation emitting particles (relativistic Doppler broadening). The line may also be created in a plasma (or corona) close to the central black hole. The line shape in this case is intrinsically Gaussian, the line energy depends on the dominant ionization states and the line width depends on rotation and Compton scattering in the corona (Kallman & White 1989).

In this paper we report the detailed spectral and temporal analyses of pointed RXTE observations of the 2003 August outburst of V4641 Sgr. In §2 we describe the general data reduction procedures adopted in this paper. In §2.1, §2.2 and §2.3 the results of the color evolution, spectral and timing analyses of the data are presented respectively. The conclusions are summarised in §3.

---

<sup>1</sup><http://ooruri.kusastro.kyoto-u.ac.jp/mailman/listinfo/vsnet-alert>

<sup>2</sup><http://www.astro.yale.edu/smarts/>

## 2. OBSERVATIONS AND RESULTS

We used optical observations of V4641 Sgr from the SMARTS consortium 1.3m telescope to trigger RXTE target of opportunity observations. The optical data were obtained using the ANDICAM (A Novel Dual Imaging CAMera, see Depoy et al. (2003) for details) instrument mounted on the SMARTS 1.3m telescope at Cerro Tololo Inter-American Observatory. The ANDICAM detector consists of a dual-channel camera that allows for simultaneous optical and IR imaging. The V band lightcurve from MJD 52840 to MJD 52870 (July 20, 2003 - Aug 19, 2003) in Fig. 1 shows rapid variability and short duration of the entire outburst, both of which are characteristic of previous outbursts of this source (Uemura et al. 2004; Wijnands & van der Klis 2000).

RXTE (Bradt, Rothschild, & Swank 1993) pointed observations of V4641 started on MJD 52856 and continued till MJD 52868 (2003 Aug 5 - 2003 Aug 17). The observable X-ray activity ceased after MJD 52858 (Aug 7, see Fig.1). Between Aug 5 and Aug 7, four RXTE pointed observations were done. A list of observation start times and durations is given in Table 1.

*HEASOFT FTOOLS* (v5.3) software was used to perform the X-ray data reduction. PCA *Science Array* data-mode with 16s time bins were used for color analysis and spectral data extraction. We extracted the lightcurves and spectral information from the top layer of the second proportional counter unit (PCU2) using the *Standard 2* files. Standard screening criteria as described in the RXTE *Cookbook*<sup>3</sup> were applied to select segments of good data when (1) the source was at least 10 degrees away from earth's limb and (2) the satellite was not passing through the region of South Atlantic Anomaly and (3) the pointing was stable with pointing offsets less than 0.02 degrees. Since the source was not very bright, we also excluded regions with significant electron contamination ( $ELECTRON2 < 0.1$ ). The errors in count-rates and hardnesses are  $1\sigma$  errors assuming a Poissonian distribution for the recorded photon count-rates. Background spectra were estimated from the latest models<sup>4</sup> using *pcabackest* (v3.0) tool. *Pcarsp* (v8.0) was used to generate the redistribution matrix files (rmf) and ancillary response files (arf) and then combined to form a single response file (rsp). We used the HEXTE *Archive* mode data from cluster A with 64 energy channels for total energy band 15-250 keV with a timing resolution of 16s. While fitting simultaneous PCA+HEXTE spectra, the normalization of the HEXTE data were left as a free parameter to match the PCA spectra.

---

<sup>3</sup>[http://rxte.gsfc.nasa.gov/docs/xte/recipes/cook\\_book.html](http://rxte.gsfc.nasa.gov/docs/xte/recipes/cook_book.html)

<sup>4</sup>[http://heasarc.gsfc.nasa.gov/docs/xte/pca\\_news.html#quick\\_table](http://heasarc.gsfc.nasa.gov/docs/xte/pca_news.html#quick_table)

Temporal information was extracted either from the *Science Event* files with  $2^{-13}\mu\text{s}$  ( $\sim 122\mu\text{s}$ ) time resolution ( $\text{DATAMODE} = E\_125us\_64M\_0\_1s$ ) or from *GoodXenon* modes of time resolution  $2^{-20}\mu\text{s}$  ( $\sim 0.95\mu\text{s}$ ), whichever available. However for the third pointing, we used the *E\\_16us\\_16B\\_36\\_1s* datamode which covers almost the entire PCA energy spectrum from 14.9 keV and above with a timing resolution of  $2^{-16}\mu\text{s}$  ( $\sim 15.2\mu\text{s}$ ) and readout time of 1s, since no event data with full PCA energy range were taken for this dwell. Data from all the detectors and their layers were combined. The event data for all the dwells were binned to  $2^{-13}\mu\text{s}$  time bins (corresponding to a Nyquist frequency of 4096 Hz) to ensure uniform analysis. Temporal studies were done in the Fourier domain using the *powspec* (v1.0) tool to carry out the Fast-Fourier Transforms and create the power density spectra (PDS) following the prescription of van der Klis (1989, 1995). Since the count-rates were not high, the dead-time effect is negligible and we did not explicitly correct the light curves for dead time. Instead we modelled the dead-time modified Poisson noise in the PDS with a constant and subtracted this constant to calculate the Fourier power. The PDS were normalized w.r.t count-rate so that the resulting power spectra are in the units of  $(\text{rms}/\text{mean})^2/\text{Hz}$ . The PDS were then logarithmically rebinned in frequency space to reduce noise at high frequencies. Unless otherwise stated, the error bars in the average power spectra were calculated by evaluating the standard deviation of the average power for each frequency. However the error bars for the individual 64s power spectra during dwell (2) were calculated by propagating through theoretical error bars obtained from the relevant chi-square distribution. The errors in spectral and temporal model fits are 90% confidence regions for a single parameter ( $\Delta\chi^2 = 2.706$ ).

## 2.1. Lightcurve and Colors

The PCA lightcurves and (5.3-10.3 keV)/(2.0-5.3 keV) color for the observed dwells are shown in Fig. 2. Here we see the highly variable nature of this source. Intensity variations by an order of magnitude in timescales as short as minutes are seen. In dwell (3) the observed count-rates were the lowest of the four dwells presented in this paper. In contrast, the immediately succeeding pointing, viz. the fourth dwell, shows the highest count-rates. While the starting time of the fourth dwell is only 1.5 hours after the ending time of the third dwell, the average count-rate of the source increased by a factor of 8.4 compared to dwell (3) and the peak count-rate is 14.4 times larger than that of dwell (3). During the fourth dwell, simultaneous optical observations of the source were done from Lu-Lin Observatory in Taiwan which showed strong X-ray/optical correlation and delayed arrival of the optical light (Bailyn et al. 2005; Maitra et al. 2004). Also, of all the RXTE pointings during this outburst, this is the last dwell where we observed any activity from the source (see Fig 1).

Contrary to what is generally observed in XRBs, the count-rates in the medium energy band (5.3-10.3 keV) are greater than that of the soft energy band (2.0-5.3 keV). This is due to the extremely strong and wide Iron emission line flux near 6.5 keV. As shown in Fig. 3(left panel), the hardness ratios (colors) do not evolve significantly during dwells (1), (3) and (4), suggesting that the overall spectral state of the source did not change during these dwells. There is a slight softening at highest luminosities during the fourth dwell which is due to the appearance of an otherwise obscured soft disc photons and is discussed in detail in §2.2. As seen in the lightcurves, the second dwell is highly dynamic in character. The hardness-time and color-color plots show that the spectral characteristics of the two flares are intrinsically very different. While the first flare near 200s is very hard in nature, the second flare near 450s is predominantly soft. The two flares occupy different regions of the color-color space, whereas the non-flaring state is distinct from either of the flaring states. There seems to be no major spectral state changes after the second flare. There is some overlap between the soft, hard as well as non-flaring state in color-luminosity space. The non-flaring state in this dwell is spectrally somewhat harder than that of the other dwells.

## 2.2. Spectroscopy

Since the spectral state of the source did not change appreciably during dwells (1), (3) and (4), we analyzed time averaged spectral and temporal properties of each of these dwells. The most notable feature in the combined spectrum is the strong, broad emission line complex around 6.5 keV which is easily seen in the counts spectrum in Fig. 4. Since such a strong line makes determination of continuum parameters difficult, we initially modelled the spectral region harder than 10 keV, with the assumption that this region is free from strong emission/absorption features or edges. For most BHXRB systems, these energy ranges are dominated by powerlaw photons. However, in this case we found that a simple powerlaw model fails to describe the spectrum (e.g.  $\chi^2/\nu = 140/45$ ). An appreciable amount of curvature was observed in the residuals, shown in Fig. 5(a), which is usually taken to be a reflection effect. We therefore used the *pexrav* model by Magdziarz & Zdziarski (1995) which calculates an exponentially cut off power law spectrum reflected from neutral material. This model provides a much better fit to the data with  $\chi^2/\nu = 35/44$  as shown in Fig. 5(b). However, the scaling factor for reflection is not well constrained by the fit and was therefore fixed to 1.0 (corresponding to an isotropic source above the disk). The overall PCA and HEXTE 3-50 keV spectrum was modelled using a warm photoelectric absorber (Morrison & McCammon 1983) of hydrogen column density fixed to  $2.3 \times 10^{21}$  atoms/cm<sup>2</sup> (Dickey & Lockman 1990) and the Comptonized powerlaw. The abundances were taken from the table by Anders & Grevesse (1989). Modelling the Fe line complex for dwell (1) required two

Gaussians, most likely corresponding to different ionization states of iron. The moderate energy resolution of the spectrometer makes it difficult to determine the exact ionization states of these lines. We tried the relativistic line model by Laor (1991) to fit the Fe  $K\alpha$  line. The Laor line energy comes out to be similar to that obtained using a Gaussian model. However other Laor fit parameters like the disc inner radius or the power law dependence of emissivity are not constrained by the data. We therefore used the simple Gaussian model for the line. For all other dwells too, single Gaussian model gave good fits to the data. The relevant free parameters in this model, besides the normalizations for the model components, are the line energies and widths of the Gaussians, powerlaw photon index and the energy of exponential cutoff. The results of the spectral deconvolution are shown in Table 2. Also shown in Table 2 are the values of reduced chi-squares obtained for the best fit model and the corresponding 3-50 keV isotropic luminosity for a distance of 10 kpc. (also see Fig. 4).

Since the broad colors show sharp spectral state changes during the second dwell, we have not attempted to create any time averaged spectrum of the entire dwell. Instead we present a dynamic energy spectrum (DES, Fig. 6) which shows the spectral evolution of the source during this dwell. To create the DES we extracted 69 spectra spanning the entire dwell with timing resolution of 32 seconds. The spectra were then normalized by count-rate. We also extracted the entire time averaged spectrum for the whole dwell and normalized by count-rate. This normalized, time averaged spectrum of the entire dwell was used as a template spectrum. Each 32s spectrum was divided by the template spectrum and the resulting ratio spectrum constitutes a vertical strip in the DES. The color coding corresponds to the ratio of observed spectrum to the template spectrum at the time (abscissa) for the energy (ordinate). The overplotted solid histogram shows the variation of PCA 3-20 keV lightcurve during the dwell. It is evident from the DES that the flares during 200s and 450s are intrinsically different in their spectral natures. The first flare near 200s is very hard with a sharp dropout of soft photons whereas the second flare near 450s is essentially soft in nature. As in the previous dwell, we do not find any significant blackbody component in the spectra. The 3-25 keV spectra are dominated by an iron emission line and powerlaw continuum. We modelled the 10-25 keV spectra during the first 14-94 seconds of the dwell, i.e. *before* the hard flare, using the pexrav model. In Fig. 7(a) we show the corresponding spectrum and the fit. The solid histogram is the Comptonized powerlaw fit to the hard 10-25 keV data which does not account for the broad Fe  $K\alpha$  emission line seen in the data near 6.5 keV. Therefore, as expected, when extrapolated to lower energies, the model is unable to reproduce the strong iron line near 6.5 keV but the fit matches the continuum well at the lowest energies. In sharp contrast to this is the spectrum *during* the hard flare (222-254 seconds), shown in Fig. 7(b). The solid histogram, as before, is a Comptonized powerlaw

fit to the 10-25 keV energy range which is not only unable to reproduce the region near the iron line complex, but also largely overestimates the soft photon count-rate in the 2-5 keV range.

In fact, the spectrum during the hard flare can not be modelled using any physical model if the column density of the absorber is fixed to its standard value of  $2.3 \times 10^{21} \text{ atoms/cm}^2$  (Dickey & Lockman 1990). In contrast, the spectrum before and after the flare can be well modelled using this standard column density. We therefore allowed the fit parameter  $n_H$  which estimates the column density of the warm absorber to vary during the flare. A comptonized powerlaw (Magdziarz & Zdziarski 1995) was used for the continuum and a gaussian for the Fe line. In this model, the variation of the fit parameter  $n_H$ , with time, is shown in Fig. 8. Due to low count rates and moderate resolution of the spectrometer it is difficult to determine precisely the column density of the warm absorber, our 90% confidence range on the estimated maximum column density during the hard flare is  $(78.3 \pm 12.9) \times 10^{22} \text{ atoms/cm}^2$ , almost 2 orders of magnitude greater than the rest of the dwell. One possible physical scenario that could lead to such an event is the eruption of a hard jet followed by an enhanced outflow of mass, as also envisioned by Revnivtsev et al. (2002). Such an outflow moving nearly along the line of sight can cause such large changes in observed column density. Other scenarios like variation of partial covering fraction cannot be ruled out. As regards the strong iron emission line, it is likely that the source is obscured and the circumstellar material is excited by hard X-ray emission, which in turn produces the line emission with strong equivalent widths.

The 10-50 keV hard energy spectrum for the third dwell could be well described by a simple powerlaw ( $\chi^2/\nu = 33.7/45$ ). Unlike the previous dwells, the data for the third dwell did not require any Comptonization component. Most likely, this is due to the low count-rates and associated larger errorbars which makes detection of reflection component difficult. At lower energies, the data do not require any thermal disc photons. However, the column density of the absorbing column was larger than the standard value, during the entire third dwell, which could be possible if the observation was made shortly after a (possibly super-Eddington) mass ejection event. An absorption edge near 10 keV in terms of a smeared edge model (Ebisawa et al. 1994) was also required. The width of the smeared edge was fixed to 10keV.

For the fourth dwell, which was the brightest of all the four pointings, the HEXTE spectrum was seen to extend up to 150 keV. In Fig.10 we show the 3-150 keV PCA+HEXTE spectrum. Although the lightcurve showed a variation in flux of an order of magnitude over the entire dwell, the X-ray colors or a DES shows that the spectral state of the source did not change during first 1000 seconds of the dwell. During the 1000-1200 seconds, it

appears that the source went through another faint hard flare as seen in dwell (2). Unlike the other dwells, the spectra for this dwell however shows an excess of soft photons, most likely from an accretion disk. A smeared edge near 10keV was also required. A simple model with a Gaussian line and two continuum components, viz. a multicolor disk (Mitsuda et al. 1984; Shakura & Sunyaev 1973) and a Comptonized powerlaw (Magdziarz & Zdziarski 1995) gives a very high temperature of the inner edge of the accretion disk of around 3.3 keV. Assuming a Comptonized blackbody model (*compbb*, see Nishimura et al. (1986) for details) with an electron temperature of the hot plasma fixed to 20 keV and a Comptonized powerlaw with fixed photon index of 1.5 and cutoff at 150 keV, better fits are obtained ( $\chi^2/\nu = 75.4/80$ , also see Fig. 10) and lower temperature of the blackbody ( $\sim 1.9$  keV). The fitted parameter values for the model are given in Table 2. However the *compbb* model assumes a single temperature blackbody emission as a seed photon spectrum whereas in reality, the seed photons most likely are coming from an accretion disk with a varying temperature profile. Small systematic deviations are seen in the plot of residuals (bottom panel of Fig. 10) and could be fitted by adding more models components, but due to lack of a thorough understanding of actual undergoing physical processes we constrained ourselves to simple models.

### 2.3. Temporal analysis

The rapid state changes seen in the energy spectra during the second dwell also left strong signatures in temporal domain. The rms variability with time, during the second dwell, in the soft (2.4-4.1 keV), Fe line complex (5.3-7.8 keV) and hard (14.9-25.0 keV) energy bands show significant changes (Fig 9). The total rms variability in 0.1-10 Hz range was calculated for every 64 second long data segments. We see that the line variability tracks the soft variability throughout the dwell. Therefore it is unlikely that any of these flares is caused solely by the variability in the line. Note that the variability increases to a maximum near the hard flare (near 200s) for all energy bands which may be caused by an outflow crossing the observer's line of sight, where the ejected matter has a high rms variability. An enhancement in the Comptonizing corona that surrounds the source and gives rise to the high variability hard photons (e.g in low/hard states of most compact X-ray binaries) could also account for the increase in variability.

Interestingly, we see no change in hard band variability during the soft flaring event near 450s, but both the soft and the line flux variabilities go through a large increase in variability during the flare. A dip in the hard band variability is seen after the soft flaring event. The hard flaring event could cause instability in the circumstellar environment of

the source causing a decrease in optical depth of the corona and thereby allowing larger number of scattered soft disk photons to reach the observer. Thus the soft flare may be due to the appearance of a brief ‘window’ in the obscuring circumstellar material, allowing us a glimpse of the inner regions. The soft-band variability drops just after the soft flare while the hard-band variability slowly increases suggesting the rebuilding of the obscuring corona/circumstellar material. After the flare around 800s, the source activity decreased and we see no significant evolution in spectral or temporal domains.

For the remaining dwells, viz. (1), (3) and (4), the PDS show little or no rms variability in the frequency range of 0.1-10.0 Hz, in any of the soft, Fe line complex or hard (14.9-25.0 keV) energy regimes. This suggests no temporal variability in 0.1-10 Hz range over the 2.5-25 keV energy range during the entire observation. We therefore constructed a white (2.5-25 keV) PDS over the entire dwell. Below  $\sim 1$  Hz the PDS is essentially dominated by featureless red noise with little or no signature of any peaked noise. There might be some evidence of a flat-topped noise at the lowest frequencies ( $< 0.01$  Hz) but it is not statistically significant from the data. Above a few Hz the spectrum is dominated by Poisson noise. In Table 2 we present the rms variability seen in the 2.5-25 keV photons, as a Riemann sum of frequencies between 0.01-10 Hz and the powerlaw index ( $\alpha$ ) that characterises the slope of the red noise.

### 3. Discussion

Analysis of the data presented in this paper suggests that the compact object in V4641 Sgr is enshrouded by an optically thick cloud, at least during some periods of its enhanced activity during the outburst of 2003. Optical (Charles et al. 1999) and X-ray (Revnivtsev et al. 2002) observations during the previous outbursts also suggest similar physical environment. The cloud could be composed of outflowing matter from the inner regions close to the central black hole. The strong powerlaw dominated flux seen in the observed dwells indicate that the source was in the canonical low/hard state. The energy spectrum of dwells (1)-(3) do not seem to require a soft disk blackbody component. High column density observed during the outburst can in part cause the lack of detection of the soft disk component. High orbital inclination, along with presence of gas and dust can also potentially obscure the accretion disk from the observer and this may be the case for V4641 Sgr. In a recent work, Narayan & McClintock (2005) have pointed out that the X-ray binary systems which have high inclination, show strong variability and complex, non-FRED like outbursts. The inner disk, which may be warped and combined with the modestly high inclination of the binary orbit, can have an inclination near  $90^\circ$ . Then small changes in the height of the disk could

cause rapid obscuration and changes in the observed flux, if the material is somewhat thin could cause changes in column density, and if it is thick could cause variations in the reflection component. Although no Super-Eddington events were detected in any of the dwells presented in this work, given the high variability of the source, it is possible that there were short episodes of such Super-Eddington accretion that lead to the formation of a dynamic environment around the central engine.

The color-luminosity diagram for dwell (2) shows that there is significant overlap in luminosity between the hard, soft and the non-flaring state. This supports the suggestion that the luminosity (and hence the associated inferred mass accretion rate,  $\dot{M}$ ) is not the only parameter that causes a state transition in XRBs (Homan et al. 2001; Smith et al. 2002; Maccarone & Coppi 2003; Maitra & Bailyn 2004). The data imply a second (or more) parameter determining state transition in these sources.

There is evidence for Comptonization, both from the presence of a broad Fe line complex near 6.5 keV as well as a characteristic Compton hump in  $> 10$  keV range. The Compton reflection fraction is not well constrained by the models which might be due to modification of the emergent spectra by an outflow around the source. Titarchuk & Shrader (2005) have recently shown that in a relatively cold outflow of  $T \sim 10^6$  K, emerging photons are predominantly downscattered which can lead to an accumulation of excess photons  $\sim 10$  keV. Such excess  $\sim 10$  keV was seen for V4641 Sgr and therefore strengthens the enshrouded source with an outflow model for this source. Even during periods of high luminosity, a simple multi-color disk fit gives an unrealistically high disc temperature. One possible interpretation of such high fitted disk temperatures is an existence of a hot electron cloud very near to the disk which Compton upscatters the disk photons and converts a significant fraction of the disk emission into higher energies as also observed in another black hole binary with superluminal jet, XTE J1550-564 (Kubota & Makishima 2004). The origin of broad iron emission lines with equivalent widths up to 1 keV seen during the observations could either be Compton reflection from an accretion disk or a corona. From the data we were unable to differentiate between the origin of the lines. However since other evidence favor an enshrouded source, the coronal line formation scenario seems more likely. Timing analysis shows that during all four observations the PSD were dominated by red powerlaw noise below few Hz and Poisson noise above it. Besides the powerlaw continuum or the constant Poisson level, no other features like breaks or QPOs were seen in any of the power spectra. The absence of any signal at frequencies higher than few Hertz and a featureless red noise at lower frequencies further support an enshrouded obscured source where all the high-frequency/short timescale events have been smeared out as the radiation passes through the obscuring material.

DM would like to thank Jeroen Homan and Paolo Coppi for many useful discussions.

We would also like to thank the *RXTE* team for swiftly triggering our target of opportunity observations and the SMARTS observers J. Espinoza and D. Gonzalez for taking the data and R. Winnick, who accommodated our many requests to revise the observing schedule. This work was supported by National Science Foundation grant AST 00-98421, AST 04-07063, NASA ADP grant NAG5-13336 and data analysis grant NAG5-13777. This research has made use of data obtained from the High Energy Astrophysics Science Archive Research Center (HEASARC), provided by NASA’s Goddard Space Flight Center.

## REFERENCES

- Anders, E., & Grevesse, N. 1989, *Geochim. Cosmochim. Acta*, 53, 197
- Bailyn, C., Maitra, D., Buxton, M., Jeanty, L., & Gonzalez, D. 2003, *The Astronomer’s Telegram*, 171, 1
- Bailyn, C., et al. 2005, in preparation
- Bradt, H. V., Rothschild, R. E., & Swank, J. H. 1993, *A&AS*, 97, 355
- Buxton, M., Maitra, D., Bailyn, C., Jeanty, L., & Gonzalez, D. 2003, *The Astronomer’s Telegram*, 170, 1
- Charles, P. A., Shahbaz, T., & Geballe, T. 1999, *IAU Circ.*, 7267, 2
- Chen, W., Shrader, C. R., & Livio, M. 1997, *ApJ*, 491, 312
- Depoy, D. L., et al. 2003, *Proc. SPIE*, 4841, 827
- Dickey, J. M., & Lockman, F. J. 1990, *ARA&A*, 28, 215
- Ebisawa, K., et al. 1994, *PASJ*, 46, 375
- George, I. M., & Fabian, A. C. 1991, *MNRAS*, 249, 352
- Goranskij, V. P. 1978, *Astronomicheskij Tsirkulyar*, 1024, 3
- Hjellming, R. M., & Rupen, M. P. 1995, *Nature*, 375, 464
- Hjellming, R. M., et al. 2000, *ApJ*, 544, 977
- Hjellming, R. M. 2000, *The Astronomer’s Telegram*, 61, 1

- Homan, J., Wijnands, R., van der Klis, M., Belloni, T., van Paradijs, J., Klein-Wolt, M., Fender, R., & Méndez, M. 2001, *ApJS*, 132, 377
- in 't Zand, J., Heise, J., Bazzano, A., Cocchi, M., di Ciolo, L., & Muller, J. M. 1999, *IAU Circ.*, 7119, 1
- Kallman, T., & White, N. E. 1989, *ApJ*, 341, 955
- Kubota, A., & Makishima, K. 2004, *ApJ*, 601, 428
- Laor, A. 1991, *ApJ*, 376, 90
- Maccarone, T. J., & Coppi, P. S. 2003, *MNRAS*, 338, 189
- Magdziarz, P., & Zdziarski, A. A. 1995, *MNRAS*, 273, 837
- McClintock, J. E., & Remillard, R. A., 2004, in *Compact Stellar X-Ray Sources*, ed. W. H. G. Lewin & M. van der Klis (Cambridge: Cambridge Univ. Press), in press (astro-ph/0306213)
- Maitra, D., & Bailyn, C. D. 2004, *ApJ*, 608, 444
- Maitra, D., Bailyn, C., Chen, A., Buxton, M., & Jeanty, L. 2004, *AIP Conf. Proc.* 714: X-ray Timing 2003: Rossi and Beyond, 714, 56
- Markoff, S., Falcke, H., & Fender, R. 2001, *A&A*, 372, L25
- Markwardt, C. B., Swank, J. H., & Marshall, F. E. 1999, *IAU Circ.*, 7120, 1
- Mirabel, I. F., & Rodriguez, L. F. 1994, *Nature*, 371, 46
- Morrison, R., & McCammon, D. 1983, *ApJ*, 270, 119
- Mitsuda, K., et al. 1984, *PASJ*, 36, 741
- Narayan, R., & McClintock, J. E. 2005, *ApJ*, 623, 1017
- Nishimura, J., Mitsuda, K., & Itoh, M. 1986, *PASJ*, 38, 819
- Orosz, J. A., et al. 2001, *ApJ*, 555, 489
- Revnivtsev, M., Gilfanov, M., Churazov, E., & Sunyaev, R. 2002, *A&A*, 391, 1013
- Reynolds, C. S., & Nowak, M. A. 2003, *Phys. Rep.*, 377, 389

- Rupen, M. P., Mioduszewski, A. J., & Dhawan, V. 2003, *The Astronomer’s Telegram*, 172, 1
- Shakura, N. I., & Sunyaev, R. A. 1973, *A&A*, 24, 337
- Smith, D. M., Heindl, W. A., & Swank, J. H. 2002, *ApJ*, 569, 362
- Stubbings, R., & Pearce, A. 1999, *IAU Circ.*, 7253, 1
- Sunyaev, R. A., & Titarchuk, L. G. 1980, *A&A*, 86, 121
- Swank, J. 2004, *The Astronomer’s Telegram*, 295, 1
- Tanaka, Y., & Lewin, W. H. G. 1995, 1995, in *X-Ray Binaries*, ed. W. H. G. Lewin, J. van Paradijs, & E. P. J. van den Heuvel (Cambridge: Cambridge Univ. Press), 126
- Tingay, S. J., et al. 1995, *Nature*, 374, 141
- Titarchuk, L., & Shrader, C. 2005, *ApJ*, 623, 362
- Wijnands, R. & van der Klis, M. 2000, *ApJ*, 528, L93
- Uemura, M., et al. 2002, *PASJ*, 54, 95
- Uemura, M., et al. 2004, *PASJ*, 56, 61
- van der Klis, M., 1989, in *Timing Neutron Stars*, ed. H. Ogelman and E.P.J. van den Heuvel, NATO ASI Series C 262, 27.
- van der Klis, M., 1995, in *X-Ray Binaries*, ed. W. H. G. Lewin, J. van Paradijs, & E. P. J. van den Heuvel (Cambridge: Cambridge Univ. Press), 252

Table 1. Observation Log

Serial Number	ObsID	Calendar Date (dd-mm-yyyy)	Time <sup>a</sup> (MJD)	Exposure <sup>b</sup> (seconds)
1	80054-08-01-00	05-08-2003	52856.06	992
2	80054-08-01-01	06-08-2003	52857.37	2192
3	80054-08-02-00	07-08-2003	52858.50	944
4	80054-08-02-01	07-08-2003	52858.57	1296

<sup>a</sup>Start of good time interval.

<sup>b</sup>Total exposure time after screening for good time intervals.

Table 2. Important Spectral and Temporal Fit Parameters

SPECTRAL PROPERTIES					TEMPORAL PROPERTIES			
Dwell	Model	Component	Parameter	Fitted value	Red-noise Slope	RMS(%)		
(1)	WABS× (GAUSSIAN+GAUSSIAN+PEXRAV)	Gaussian(1)	Line Energy (keV)	6.79 <sup>+0.29</sup> <sub>-0.24</sub>	-1.92 <sup>+0.27</sup> <sub>-0.25</sub>	15		
			Line width (σ, keV)	1.48 <sup>+0.24</sup> <sub>-0.18</sub>				
			Equivalent width (keV)	0.85				
		Gaussian(2)	Line Energy (keV)	6.49 <sup>+0.04</sup> <sub>-0.04</sub>				
			Line width (σ, keV)	0.24 <sup>+0.11</sup> <sub>-0.21</sub>				
			Equivalent width (keV)	1.06				
		Pexrav	Photon Index	1.01 <sup>+0.15</sup> <sub>-0.12</sub>				
			Cutoff energy (keV)	24.0 <sup>+3.4</sup> <sub>-3.1</sub>				
		$L_{3-50keV} = 1.5 \times 10^{37}(d/10kpc)^2$ ergs/s					$\chi^2/\nu = 49/55$	
		(3)	WABS× SMEDGE×(GAUSSIAN+POWERLAW)	Wabs			$n_H$ (×10 <sup>22</sup> atoms/cm <sup>2</sup> )	13.9 <sup>+2.6</sup> <sub>-2.4</sub>
Smedge	Threshold energy (keV)				10.5 <sup>+0.7</sup> <sub>-0.7</sub>			
	$\tau$			1.78 <sup>+0.58</sup> <sub>-0.55</sub>				
	Gaussian			Line energy (keV)	6.16 <sup>+0.13</sup> <sub>-0.13</sub>			
				Line width (σ, keV)	0.66 <sup>+0.21</sup> <sub>-0.22</sub>			
Powerlaw	Equivalent width (eV)			866				
	Photon index			1.64 <sup>+0.14</sup> <sub>-0.13</sub>				
	$\chi^2/\nu = 46/56$							
$L_{3-50keV} = 6.4 \times 10^{36}(d/10kpc)^2$ ergs/s								
(4) (0-1000s)	WABS× SMEDGE×(COMPBB+PEXRAV +GAUSSIAN)			Smedge	Threshold energy (keV)	9.98 <sup>+0.24</sup> <sub>-0.22</sub>	-1.46 <sup>+0.04</sup> <sub>-0.07</sub>	72
		Compbb	kT (keV)		1.96 <sup>+0.37</sup> <sub>-0.30</sub>			
			$\tau$	1.48 <sup>+0.33</sup> <sub>-0.44</sub>				
			Gaussian	Line energy (keV)	6.23 <sup>+0.35</sup> <sub>-0.35</sub>			
				Line width (σ, keV)	0.76 <sup>+0.09</sup> <sub>-0.08</sub>			
		Gaussian	Equivalent width (eV)	858				
			$\chi^2/\nu = 75/80$					
		$L_{3-50keV} = 6.3 \times 10^{37}(d/10kpc)^2$ ergs/s						



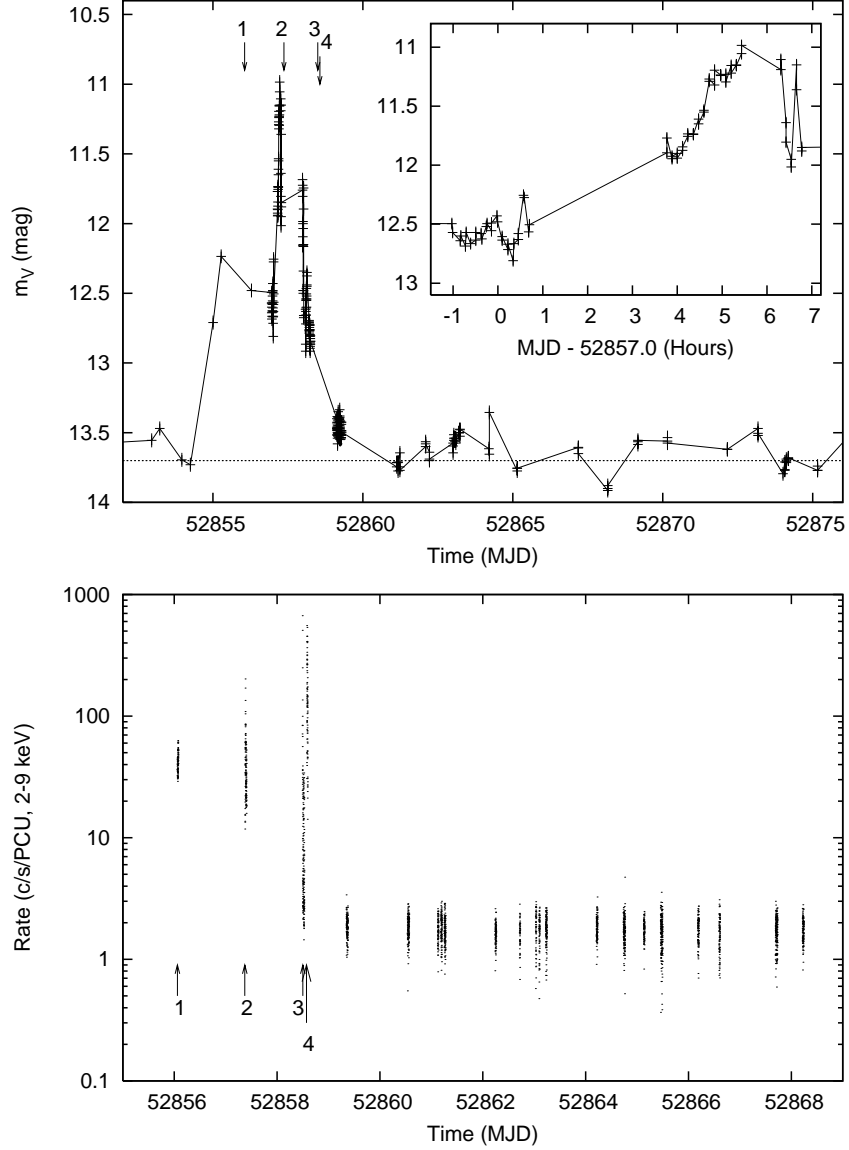


Fig. 1.— Top: V band lightcurve of V4641 Sgr during the Aug 2003 outburst. Four vertical lines on the top labelled 1-4 are the times when significant X-ray activity was observed by RXTE (see Table 1). The horizontal dotted line represents the mean quiescent brightness of 13.7 magnitude. The inset is a zoom near MJD 52857.0 to show intra-night optical variability. Bottom: X-ray activity of V4641 Sgr during the Aug 2003 outburst as seen by RXTE. The count-rates presented are 2-9 keV background subtracted rates. The four vertical lines labelled 1-4 near the bottom are the observation dwells that have been studied in this paper (see Table 1). The PCA background level is about 2 millicrab or 5.57 counts/PCU. The optical and X-ray observations shown here are not coincident. Simultaneous optical observations were obtained during dwell (4) using the NCU Lu-Lin Observatory, Taiwan and reported separately (Maitra et al. 2004; Bailyn et al. 2005).

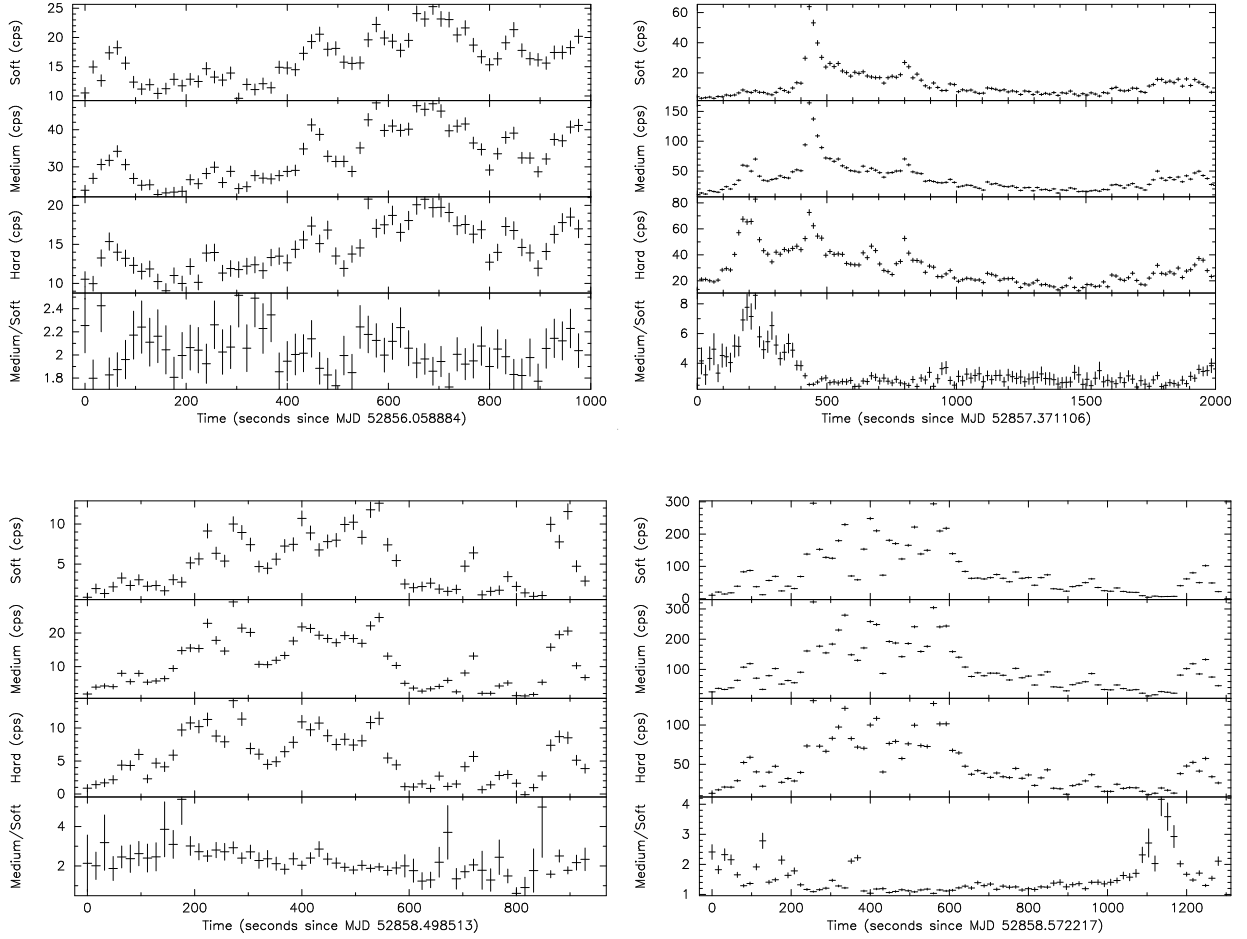


Fig. 2.— X-ray flux and hardness ratio variations with time for the observed RXTE pointings. Dwell (1) is shown on top left, dwell (2) on top right, dwell (3) on bottom left and dwell (4) on bottom right. Each dwell is subdivided in four subpanels where the top subpanels show 2.0-5.3 keV PCU2 count-rates (Soft), the second subpanels show 5.3-10.3 keV PCU2 count-rates (Medium), third shows the 10.3-20.4 keV PCU2 count-rates (Hard) and the fourth subpanels show the Medium/Soft hardness ratio.

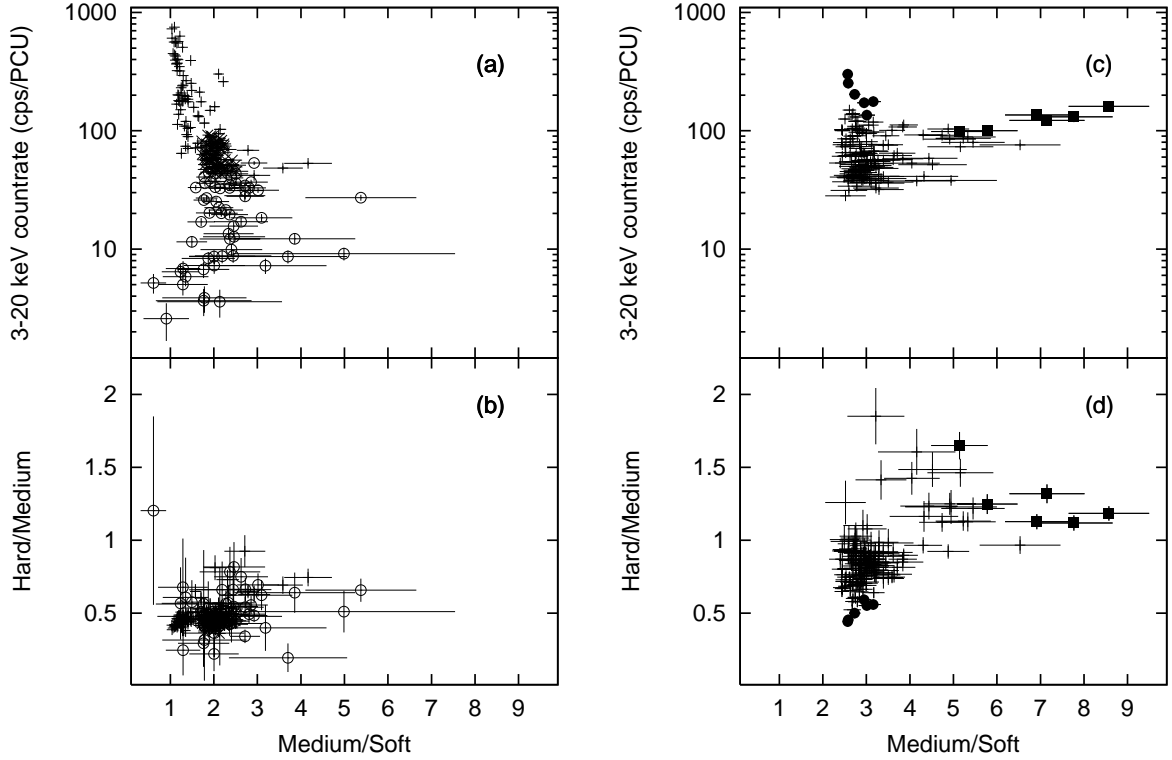


Fig. 3.— Panel (a): Medium/soft band hardness ratio is plotted against the 3-20keV background subtracted count-rates for dwells (1),(3) and (4). The corresponding color-color plot is shown in panel (b). In both plots, data from dwell (1) are shown by crosses ( $\times$ ), data from dwell (3) are shown by open circles ( $\circ$ ) and the data from dwell (4) are shown by plusses (+). In panels (c) and (d) we show the same plots as (a) and (b) respectively, but just for dwell (2) where we observed some violent hard and soft flaring activities. The data taken during the hard flare are shown by filled squares ( $\blacksquare$ ), those during the soft flare are shown by filled circles ( $\bullet$ ) and the data taken during the rest of the dwell are shown by plusses (+).

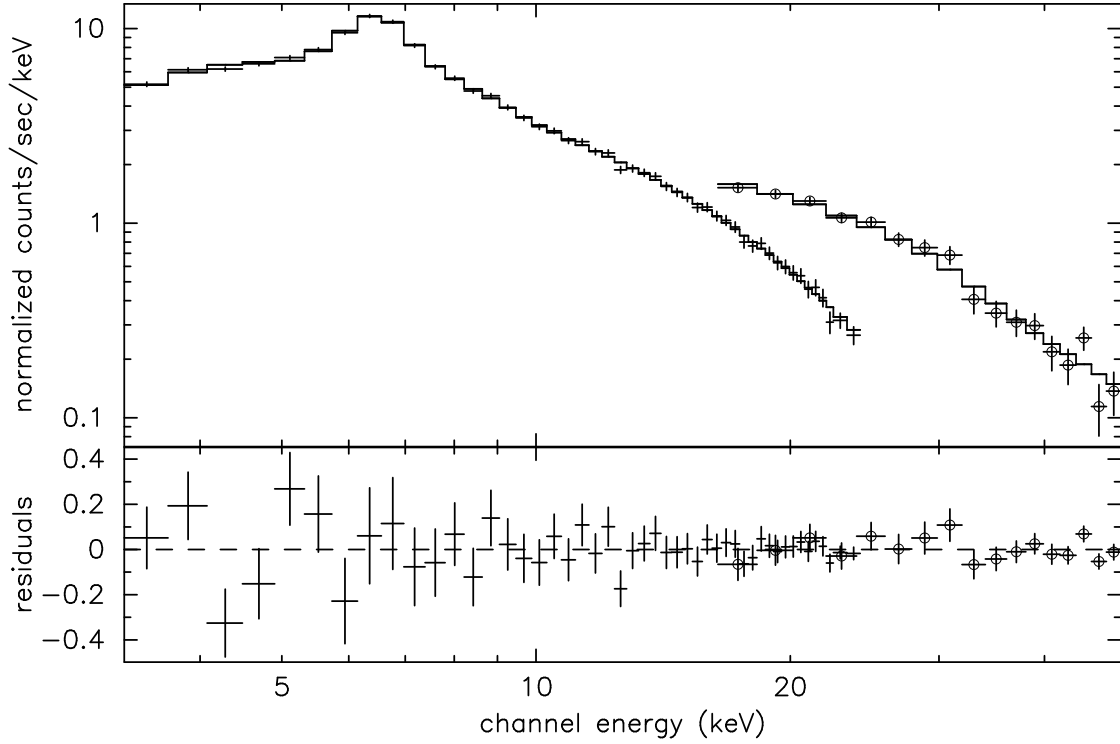


Fig. 4.— Observed count rate PCA (+) and HEXTE ( $\oplus$ ) spectrum and Comptonized spectrum model (histogram) for the average emission during dwell (1) is shown on the top panel and the residuals in the bottom panel. Note the strong Fe line feature between 6 and 7 keV.

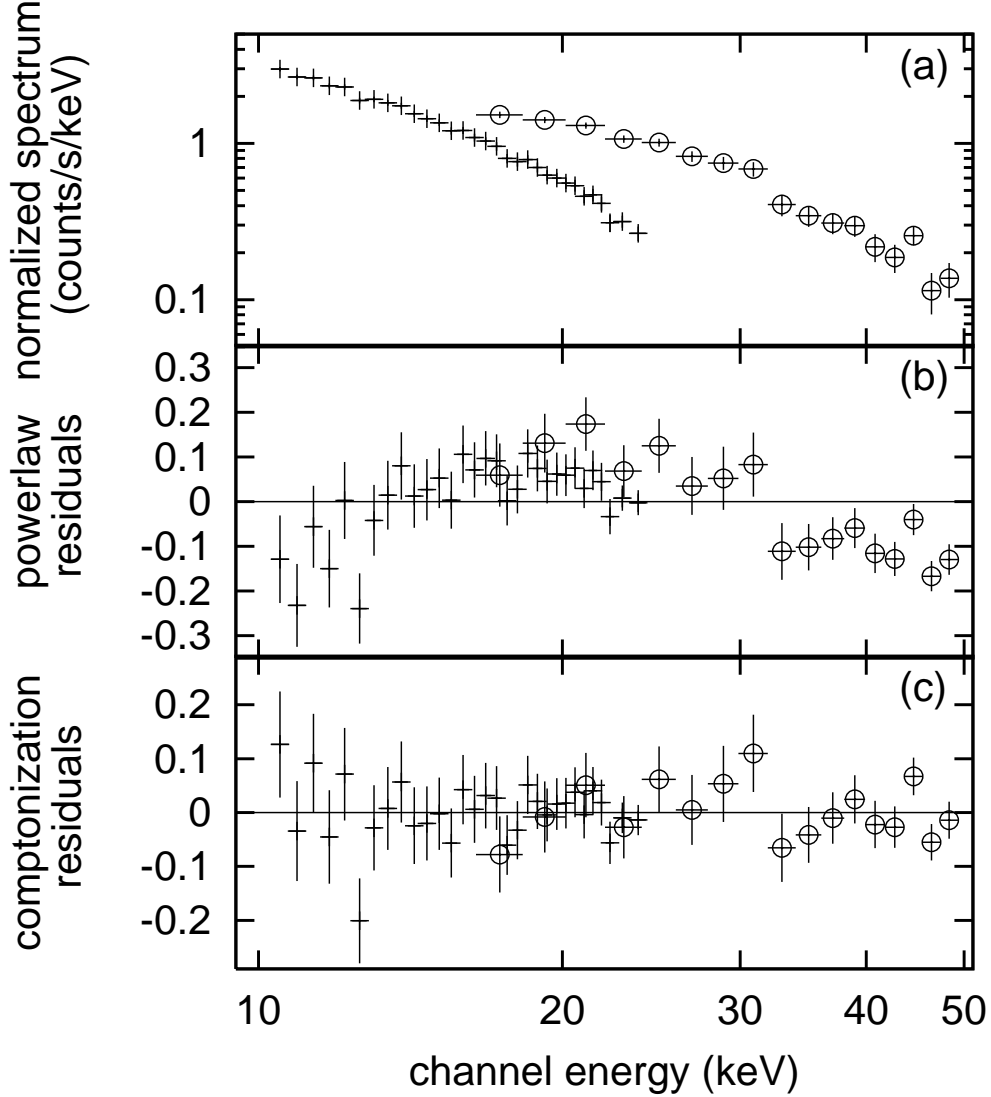


Fig. 5.— Panel (a): Time averaged counts spectrum during dwell (1). The PCA data are marked by + and HEXTE data by  $\oplus$  symbols. Panel (b): Residuals to a powerlaw fit to the energy spectrum in panel (a). Systematic deviations from a powerlaw is evident in this panel. Panel (c): Residuals to a Comptonized powerlaw fit to the same data. There is no systematic deviation, although the sharp change just above 30 keV seen in the HEXTE spectrum is still unaccounted for.

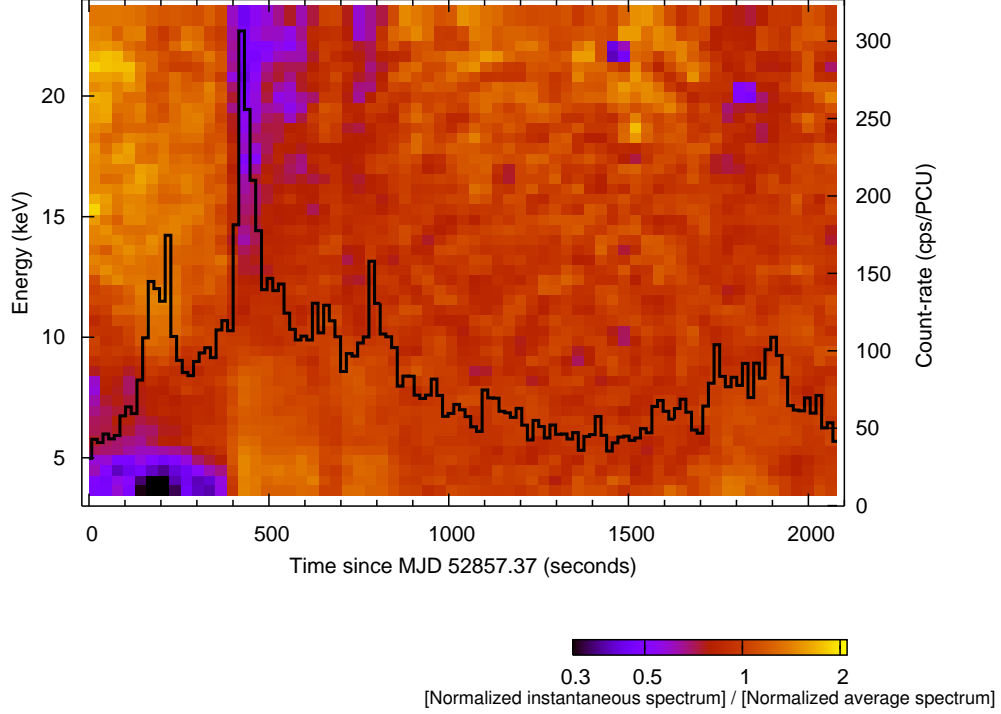


Fig. 6.— Dynamic Energy Spectrum of V4641 Sgr during dwell (2). Time variation of normalized spectral energy distribution is shown. For any time bin (each 32s long), the color represents the ratio of flux normalized spectrum extracted for that time bin divided by a template spectrum. The template spectrum is the flux normalized, time averaged spectrum of the entire dwell. Blue-black represents a dip in the spectrum compared with the template, while yellow represents a bump. The 3-20 keV PCA lightcurve is overplotted as the solid histogram. The different spectral nature of the two flares near 200s (hard flare/soft drop-out) and 450s (soft flare/hard drop-out) are evident.

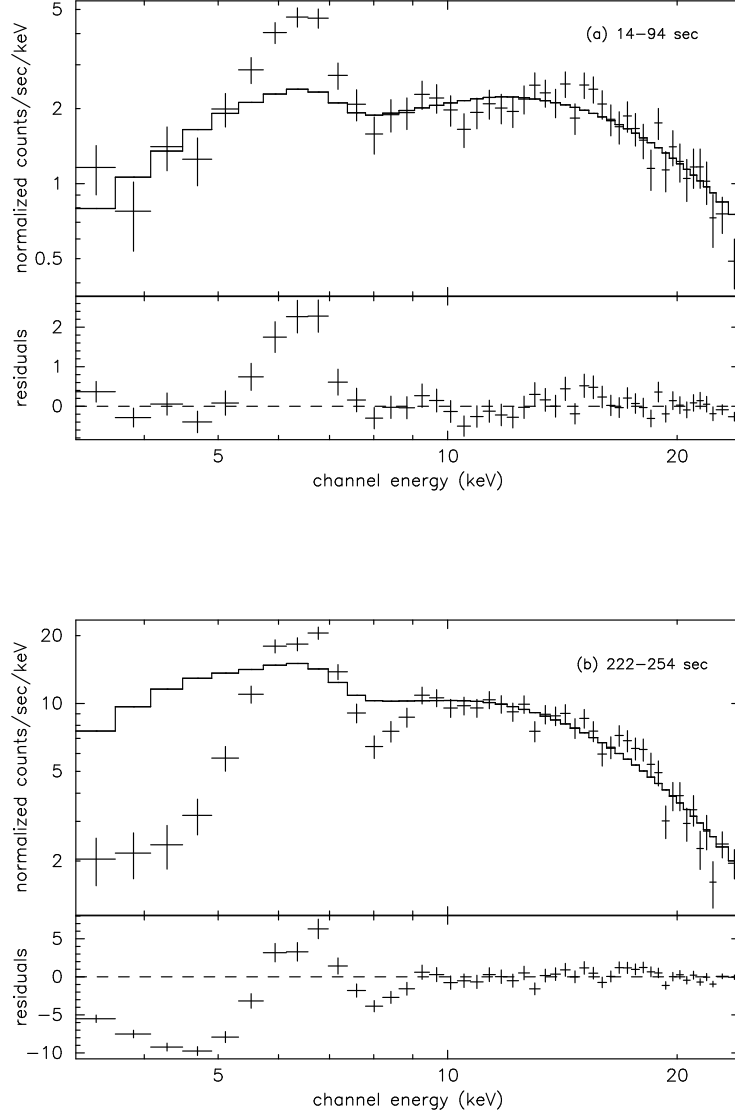


Fig. 7.— Variation of  $n_H$  during the hard flare in dwell (2). Panel (a): The energy spectrum during 14-94 seconds. Panel (b): The spectrum during 222-254 seconds when the source was going through a hard flare. The solid histogram in both panels is a fit to the 10.0-25.0 keV spectrum with  $n_H = 2.3 \times 10^{21} \text{ atoms/cm}^2$ . Note that the extrapolated fit matches the continuum at lowest energies for panel (a) whereas it grossly overestimates the counts during the flare as shown in panel (b).

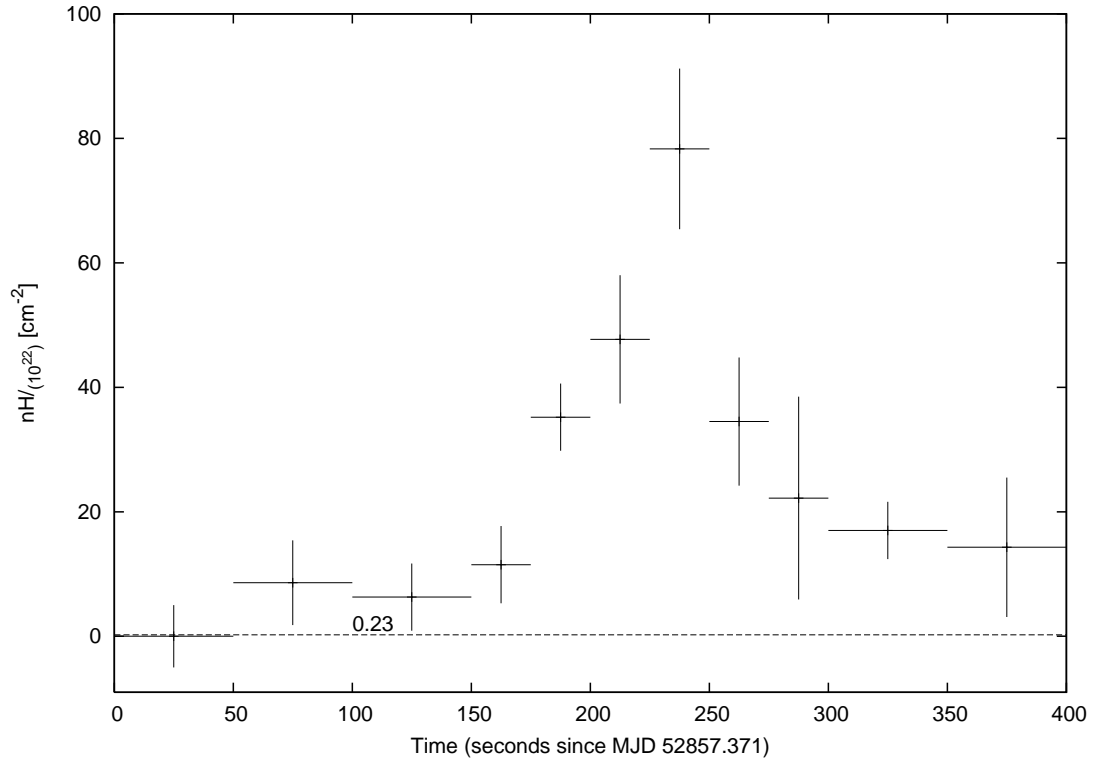


Fig. 8.— Variation of the fit parameter  $n_H$  during the hard flare. The dashed horizontal line represents the standard adopted value of  $n_H$  for this source.

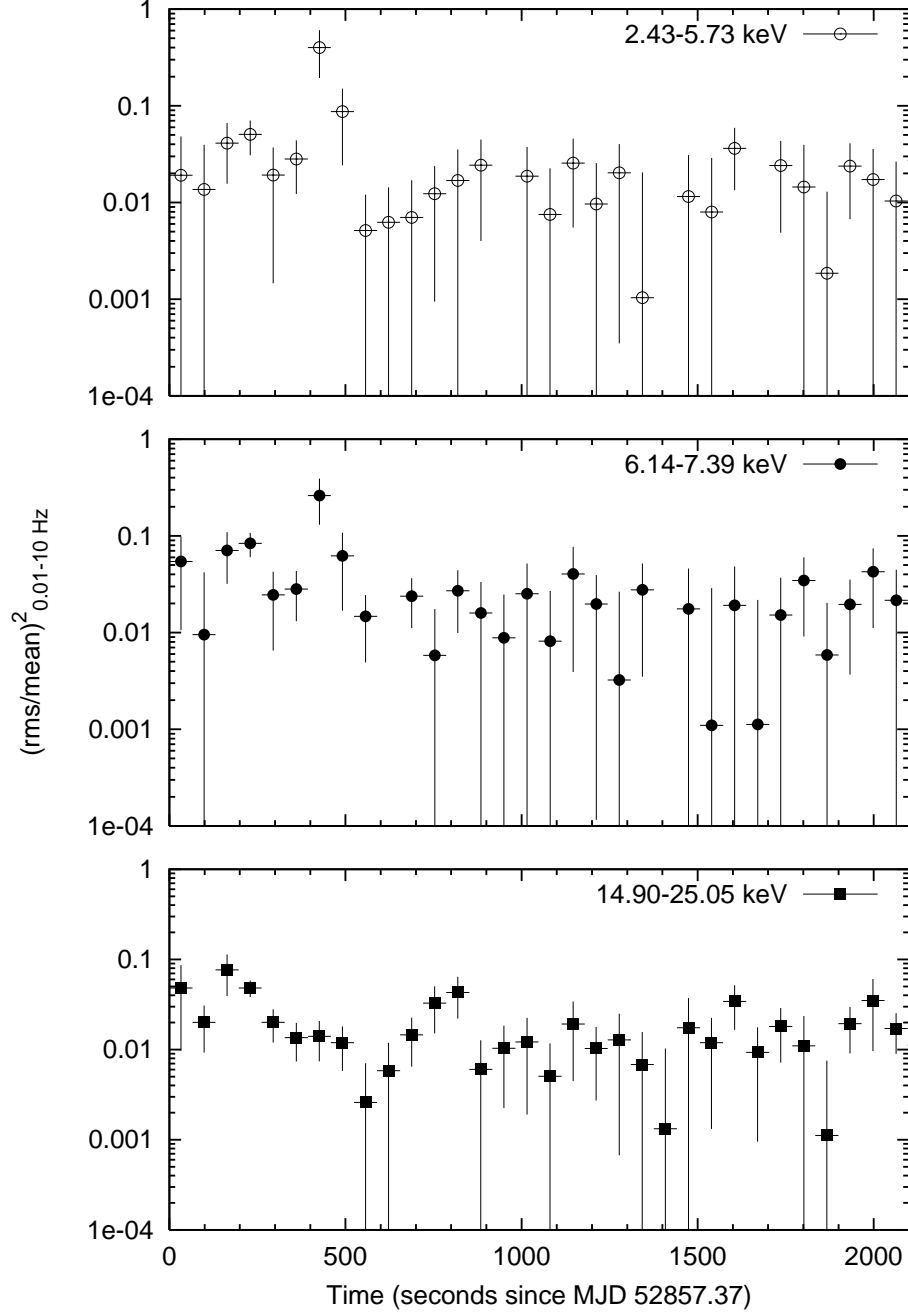


Fig. 9.— 0.01-10.0 Hz integrated RMS variability for different energy bands during dwell (2) are shown.

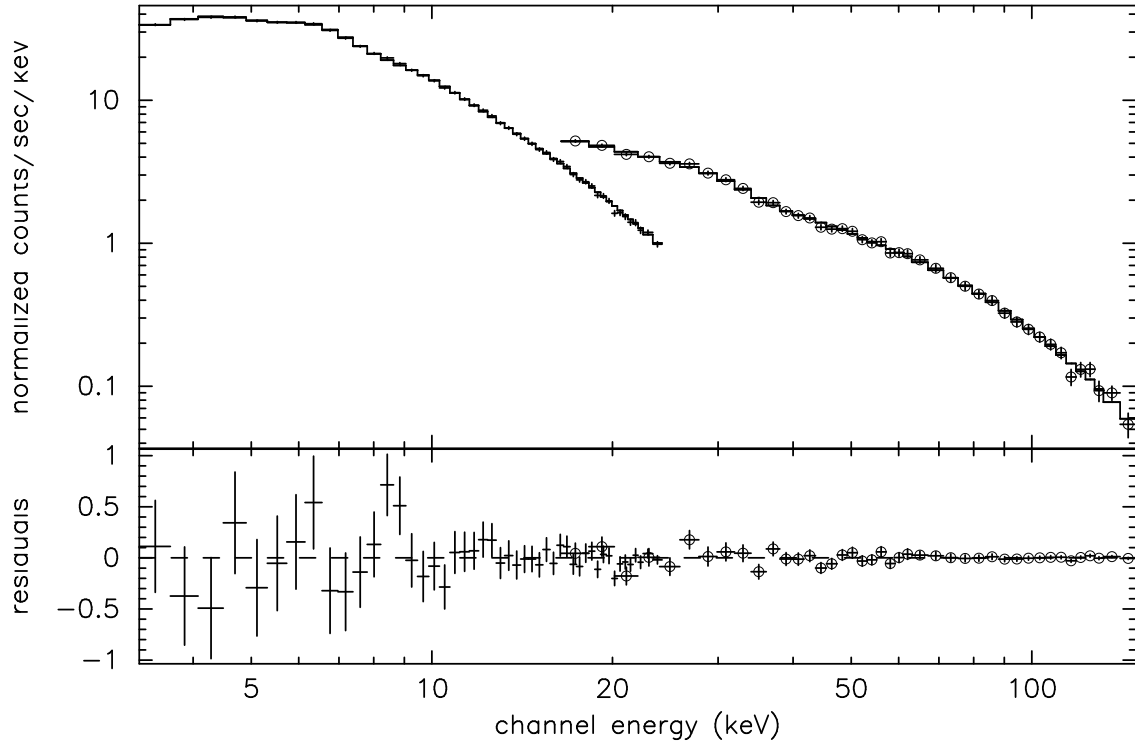


Fig. 10.— Energy spectrum during the first 1000 seconds of dwell (4). The PCA data are marked by + and HEXTE data by  $\oplus$  symbols. The model consists of a Comptonized blackbody and powerlaw to represent the continuum and a Gaussian line for the Iron  $K\alpha$  emission near 6.5 keV. A warm absorber with an  $n_H$  of  $2.3 \times 10^{23}$  atoms/cm<sup>2</sup> and a smeared edge near 10 keV is also included in the model.